AGU PUBLICATIONS

Geophysical Research Letters

RESEARCH LETTER
10.1002/2016GL071020

Key Points:
- Regional differences in the magnitude and relative contribution of extreme TWLs exist along U.S. West Coast sandy beaches
- The composition of extreme TWLs are dominated by wave runup, and the relative contribution of wave runup increases from north to south
- The relative contribution of storm surge to the still water level doubles at most locations from the annual maximum TWL to the 100 year TWL

Supporting Information:
- Supporting Information S1
- Figure S1

Correspondence to:
K. A. Serafin,
kserafin@coas.oregonstate.edu

Citation:
Serafin, K. A., P. Ruggiero, and H. F. Stockdon (2017), The relative contribution of waves, tides, and nontidal residuals to extreme total water levels on U.S. West Coast sandy beaches, *Geophys. Res. Lett.*, *44*, 1839–1847, doi:10.1002/2016GL071020

Received 2 SEP 2016
Accepted 28 JAN 2017
Accepted article online 2 FEB 2017
Published online 18 FEB 2017

The relative contribution of waves, tides, and nontidal residuals to extreme total water levels on U.S. West Coast sandy beaches

Katherine A. Serafin[1], Peter Ruggiero[1], and Hilary F. Stockdon[2]

[1]College of Earth, Ocean, and Atmospheric Sciences, Oregon State University, Corvallis, Oregon, USA, [2]St. Petersburg Coastal and Marine Science Center, United States Geological Survey, St. Petersburg, Florida, USA

Abstract To better understand how individual processes combine to cause flooding and erosion events, we investigate the relative contribution of tides, waves, and nontidal residuals to extreme total water levels (TWLs) at the shoreline of U.S. West Coast sandy beaches. Extreme TWLs, defined as the observed annual maximum event and the simulated 100 year return level event, peak in Washington, and are on average larger in Washington and Oregon than in California. The relative contribution of wave-induced and still water levels (SWL) to the 100 year TWL event is similar to that of the annual maximum event; however, the contribution of storm surge to the SWL doubles across events. Understanding the regional variability of TWLs will lead to a better understanding of how sea level rise, changes in storminess, and possible changes in the frequency of major El Niños may impact future coastal flooding and erosion along the U.S. West Coast and elsewhere.

1. Introduction

At the coast, sea level is influenced by astronomical tides, regional dynamics such as storm surges, and/or sea level anomalies coherent with the El Niño–Southern Oscillation (ENSO) [*Pugh*, 1996; *Chelton and Davis*, 1982]. High water events driven by the tide are predictable (e.g., the spring-neap cycle) due to the relative motions of the Sun, Moon, and Earth. However, normal conditions on top of background sea level rise (SLR) have already begun to produce "nuisance" flooding, or minor, recurrent flooding during high tides [*Ray and Foster*, 2016; *Sweet and Park*, 2014]. Observations of global SLR are well documented [*Church et al.*, 2013], with rates over the last century averaging 1.7 mm/yr [*Church and White*, 2011] and over the last few decades 3.4 mm/yr [*Nerem et al.*, 2010]. The combination of regional dynamics, tides, and changes in mean sea level produce spatially and temporally varying water levels [*Menéndez and Woodworth*, 2010], which will increase when considering future projections of SLR [*Tebaldi et al.*, 2012].

Water levels on beaches are further elevated by wave transformations in the surf zone through wave runup (R), a combination of wave setup and swash, which is dependent on the local wave climate [*Stockdon et al.*, 2006; *Ruggiero et al.*, 2001; *Holman and Sallenger*, 1985]. Observations of wave climate (significant wave height (Hs), peak period (Tp), and mean wave direction (MWD)) are spatially and temporally sparse, leading to records of varying completeness at any particular location. While increases in Hs in the northeast Pacific have been documented [*Young et al.*, 2011; *Ruggiero et al.*, 2010; *Méndez et al.*, 2010], projections of future changes to the wave climate [*Erikson et al.*, 2015; *Wang et al.*, 2014] are poorly constrained, leading to uncertainty in future projections of wave-induced water levels along coastlines.

This study considers total water levels (TWLs) at the shoreline of open coast, sandy beaches, defined as the superposition of wave runup, computed from an empirical formulation, and still water levels (SWL), measured from tide gauges. Coastal hazards are often dictated by TWLs crossing some threshold, e.g., the base of a dune (shown by *Stockdon et al.* [2007] using the *Sallenger* [2000] Storm Impact Scale and *Wahl et al.* [2016] and *Ruggiero et al.* [2001] using Impact Hours Per Year), where even a slight increase in the TWL may result in large changes to flooding and erosion exposure. Recent studies have suggested that the variability in coastal response to extreme water levels along the same beach may be related to the relative composition of the TWL [*Theuerkauf et al.*, 2014].

Studies have begun to consider the variation in drivers of extreme flooding events. *Dangendorf et al.* [2016] found storm Xaver brought record breaking sea levels to the coastlines of the German Bight. However, the individual processes (e.g., tides and surges) driving the event did not reach maximum elevations at coincident times, and therefore, the event was not representative of the true "worst-case" scenario for the region. The composition of coastal TWLs has been investigated by *Melet et al.* [2016] who noted that the leading contributors to TWLs in the Gulf of Guinea varied depending on the time scales considered over a 20 year period. Other studies have investigated larger-scale spatial variability in extreme SWLs to understand the contribution of tides and high- and low-frequency water levels to SWL maxima [*Merrifield et al.*, 2013; *Menéndez and Woodworth*, 2010].

Here we seek to quantify the relative contribution of waves, tides, and nontidal residuals to extreme TWLs along U.S. West Coast sandy beaches in order to better interpret drivers of coastal flooding and erosion. To do this, TWLs are calculated using a structural function approach. Daily and annual maximum events are computed for each location, and regional differences are compared. In order to examine the relative contribution from events larger than recorded (e.g., the 100 year return level event), we use the *Serafin and Ruggiero* [2014] Total Water Level Full Simulation Model (hereinafter SR14) to simulate representative synthetic records of each TWL component. The approximate 100 year TWL event is extracted from each simulation and its magnitude and makeup is compared to the annual maximum TWL event on record.

2. Methods

TWLs can be calculated by combining measured SWLs with R estimated from a model,

$$\mathrm{TWL} = \mathrm{SWL} + R. \tag{1}$$

The SWL is defined as a combination of processes, where

$$\mathrm{SWL} = \eta_{\mathrm{MSL}} + \eta_A + \eta_{\mathrm{NTR}} \tag{2}$$

and η_{MSL} is the mean sea level relative to some datum (e.g., Mean Lower Low Water (MLLW)), η_A is the astronomical tide, and η_{NTR} is the nontidal residual. The η_{NTR} can be further decomposed into

$$\eta_{\mathrm{NTR}} = \eta_{\mathrm{SE}} + \eta_{\mathrm{MMSLA}} + \eta_{\mathrm{SS}} \tag{3}$$

where η_{SE} is the intra-annual seasonal signal, η_{MMSLA} represents monthly mean sea level anomalies (interannual variability), and η_{SS} is the high-frequency residual related to storm surge due to atmospheric pressure anomalies and wind setup (see supporting information for SWL component definitions).

To compute wave runup, we use the *Stockdon et al.* [2006] empirical model, where $R_{2\%}$ is parameterized as a function of deep-water Hs, wave length (L_0), and beach slope (β). The formulation

$$R_{2\%} = 1.1\left(0.35\beta\left(H_s L_0\right)^{\frac{1}{2}} + \frac{\left[H_s L_0\left(0.563\beta^2 + 0.004\right)\right]^{\frac{1}{2}}}{2}\right) \tag{4}$$

was developed using field data from 10 experiments across 6 beaches, including data from the U.S. West Coast.

2.1. Water Level and Wave Climate Data Sets

SWLs relative to MLLW were extracted from 11 U.S. West Coast National Oceanic and Atmospheric Administration (NOAA) operated tide gauges (Figure 1a and Table S1 in the supporting information). Tide gauges were selected based on their location (approximately 200 km apart), length (record beginning at or before 1980), and completeness (95% of hourly data available). SWLs were separated into the various components η_{MSL}, η_A, and η_{NTR} (see supporting information for methods).

Each tide gauge was paired with a shelf edge, hourly wave climate extracted from an updated version of the Global Ocean Waves (GOW) reanalysis data set *Reguero et al.* [2012], most recently described and used in *Pérez et al.* [2015] (Figure 1a and Table S2). Wave hindcasts were used due to their consistent record length and shelf edge spatial resolution. The wave-induced contribution to the water level on beaches at each site was estimated by equation (4) using a uniform β in order to isolate the influence of hydrodynamic forcing

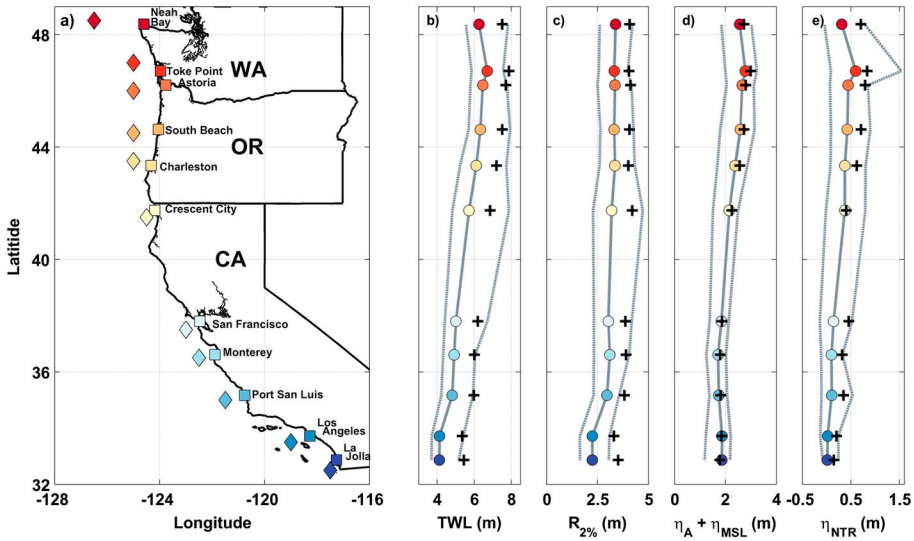

Figure 1. (a) Map of shelf edge wave hindcast nodes (diamonds) and tide gauge locations (squares). (b) Magnitude of the average (circles) and range (dashed grey line) of the annual maximum TWL event (relative to MLLW). The average (c) $R_{2\%}$, (d) $\eta_A + \eta_{MSL}$, and (e) η_{NTR} during the annual maximum TWL event. Crosses represent the magnitude of the average 100 year TWL event from simulations. Colors represent the north-to-south continuum of TWLs, where red is toward the north and blue is toward the south.

(largely driven by weather patterns) on TWLs. An estimate of $\beta = 0.05$ is based on observations from regional analyses of lidar and topographic data. Observed hourly TWL time series are over 96% complete during the time period 1979–2015 and span the U.S. West Coast from La Jolla, CA, to Neah Bay, WA.

2.2. Computation of Extreme Total Water Levels

Extreme TWLs were estimated from observational records using the annual maximum and *r* largest events [*Smith*, 1986], where *r* was defined as the top 2 through 10 events every year. Because statistics of each block of *r* largest extremes were consistent with that of the annual maximum event, observed extreme TWLs were represented by the annual maximum event. Standard methods for extrapolation of return level events include fitting models using extreme value distributions. However, while this method provides an estimated magnitude of the most extreme events, it contains no information about the constitutive processes that make up the event. To estimate the magnitude of the individual components, we generate multiple synthetic TWL records using SR14 which allows for the direct empirical extraction of return level events. Results are presented as averages and ranges of the extracted annual maximum events from the observational data and the one hundred, 100 year return level events from each simulation at every location.

2.3. Extreme Total Water Level Simulations

Simulation methods, briefly described below, follow SR14 but include extensions detailed in the supporting information [*Serafin and Ruggiero*, 2014; *Bromirski et al.*, 2003]. Using the Peak-Over-Threshold method [*Coles*, 2001], extremes are selected from time series of declustered, daily maxima Hs and η_{SS}. Independent extremes are modeled using multivariate, nonstationary Generalized Pareto distributions that include the effects of seasonality through the use of harmonics and climate variability (e.g., ENSO) via regional climate indices included as covariates [e.g., *Méndez et al.*, 2007, 2006]. Nonextreme estimates of Hs and η_{SS} are sampled from best fit monthly probability distributions. This simulation technique allows for alternate realizations of combinations of individual TWL components in order to identify various sets of physically plausible events that may not yet have been physically realized.

3. Results

3.1. Regional Variability of Total Water Levels

A clear regional variability exists in both the magnitude and composition of daily maximum TWLs along U.S. West Coast sandy beaches. Overall, daily maximum TWLs are higher in elevation, have a larger variance, and a more right-skewed distribution in Washington and Oregon than in California (Figure 2a). Regional differences in TWL distributions can be decomposed into SWL and $R_{2\%}$ (Figures 2b and 2c). The largest TWL elevations are

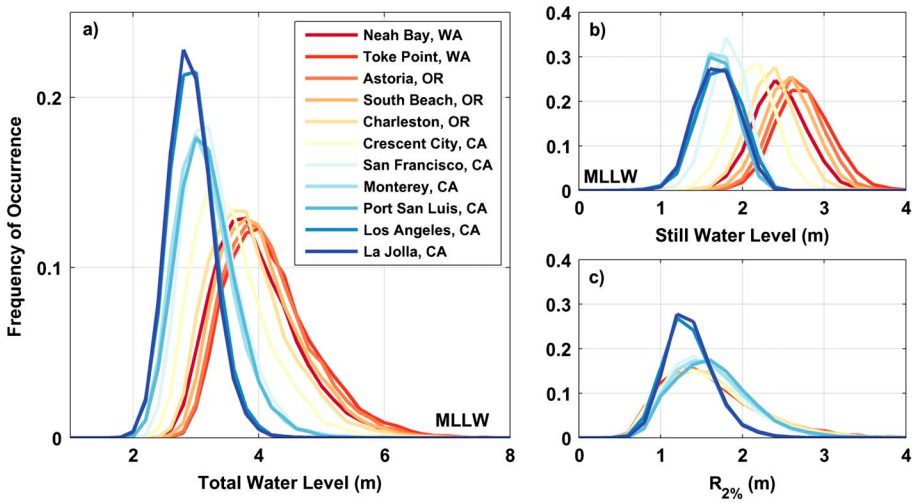

Figure 2. Distribution of daily maximum (a) TWL, (b) SWL, and (c) $R_{2\%}$ during the observed daily maximum TWL across the U.S. West Coast.

at Toke Point, WA and TWLs gradually decrease toward the south. The median of the SWL occurring during the daily maximum TWL ranges from 2.7 m (Toke Point) to 1.6 m (La Jolla, CA). The variance ranges from 5 to 12 cm, but on average is 8 cm. The median of the $R_{2\%}$ ranges from 1.5 m (Port San Luis, CA) to 1.2 m (Los Angeles, CA), while the variance ranges from 9 to 30 cm (on average 25 cm). These results demonstrate that the median of the TWL is largely dictated by the SWL, while the variance and tail behavior is dictated by the $R_{2\%}$ distribution.

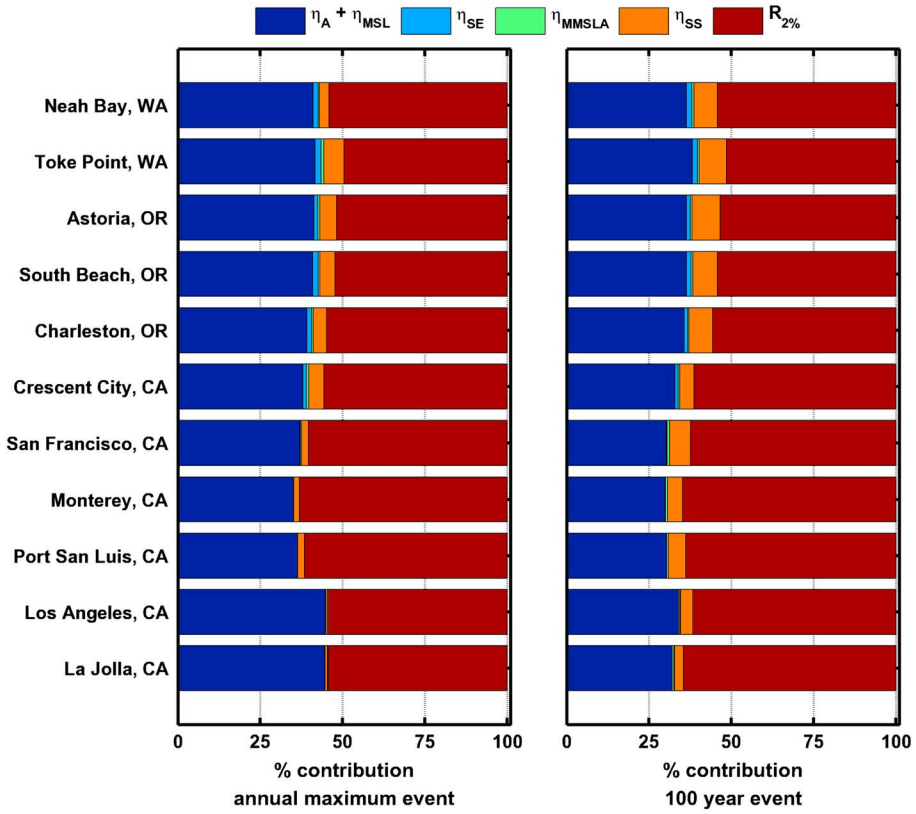

Figure 3. Relative contribution of the individual components to the annual maximum and 100 year TWL event. Bars are plotted from north (Neah Bay, WA) to south (La Jolla, CA). Red represents the wave-driven ($R_{2\%}$) component, while all other colors represent the SWL.

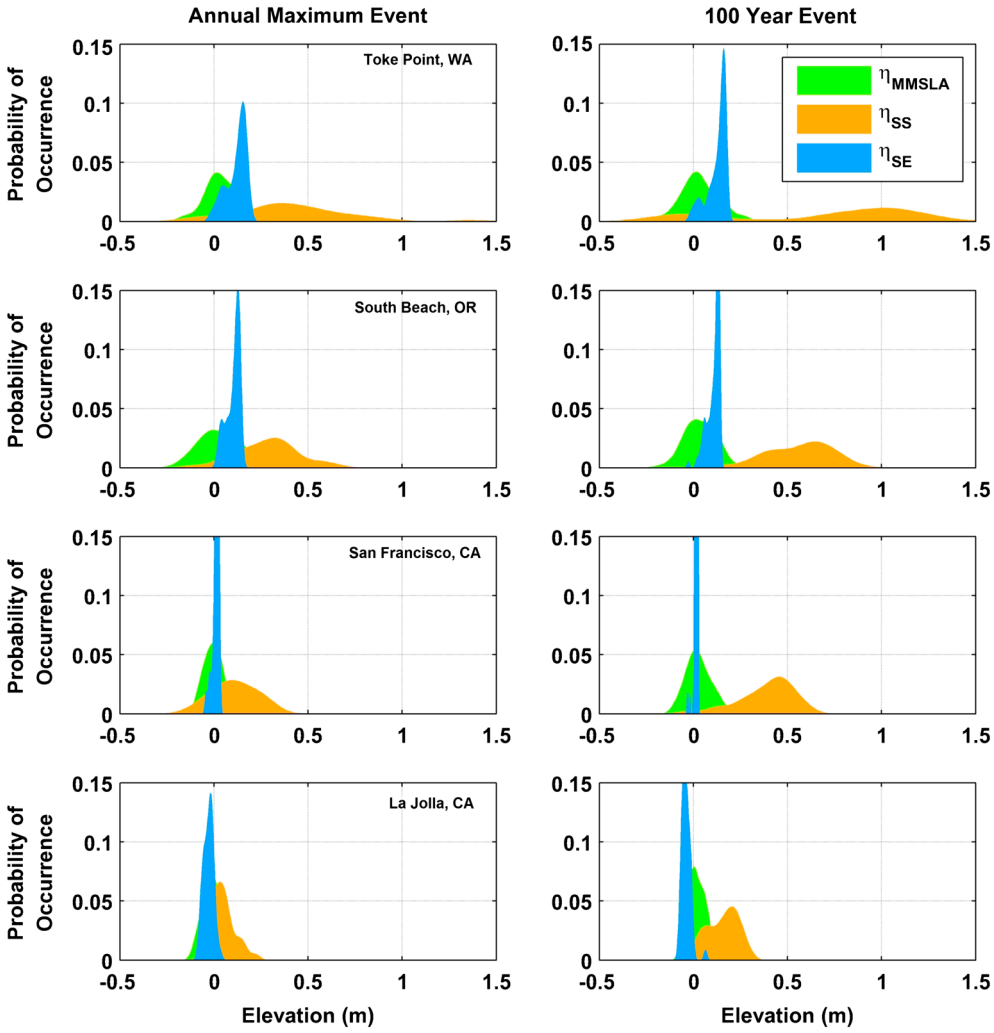

Figure 4. Distributions of the individual components that comprise the η_{NTR} during the (left column) annual maximum and (right column) 100 year TWL event.

3.1.1. Magnitude of Extreme Total Water Level Events

The average annual maximum TWL event (Figure 1b) exhibits a latitudinal variation similar to that of the daily maximum TWLs; TWLs are the largest at Toke Point, decrease toward the south and north, and extreme TWLs in California are statistically different than those in Washington and Oregon. The annual maximum TWL at Toke Point is coincident with a peak in η_{NTR} elevation, while the peak in $R_{2\%}$ occurs slightly south (in Astoria, OR; Figure 1c). In southern California, where the annual maximum TWL is lowest, the magnitude of η_{NTR} contributing to the annual maximum event is negligible, and the $R_{2\%}$ is the lowest magnitude of all stations (Figures 1c and 1e). The magnitude of $\eta_A + \eta_{MSL}$ decreases by approximately 1 m moving north to south (Figure 1d).

The 100 year TWL event is also the largest at Toke Point and decreases toward the south and slightly toward the north (Figure 1b). On average, the 100 year TWL event is 1.2 m (20%) larger than the annual maximum event at all locations. The elevation of the $R_{2\%}$ during the 100 year TWL event is approximately 40% larger than the $R_{2\%}$ during the annual maximum TWL event. In comparison, the elevation of $\eta_A + \eta_{MSL}$ increases by 1–20 cm (approximately 5%) and the elevation of η_{NTRs} increase by 3–40 cm across all locations (>100%).

3.1.2. Relative Contributions to Extreme Total Water Level Events

The relative contribution of waves and still water levels to the annual maximum TWL event is on average (± SD) 56.0% (±4.3%) R_2% and 44.0% (±4.2%) SWL across all stations. The relative contribution shifts slightly toward the $R_{2\%}$ during the 100 year TWL event which is composed of 59.0% (±5.1%) $R_{2\%}$ and 41.0% (±5.1%) SWL. A latitudinal gradient in the percent contribution of the $R_{2\%}$ exists where $R_{2\%}$ increases toward the south by 5–10% for both the annual maximum and 100 year TWL event (Figure 3).

The relative contribution of $R_{2\%}$ and SWL to the TWL slightly varies between the annual maximum and 100 year TWL event. However, the composition of the SWL is different between extreme events. During the annual maximum event, on average, 9.5% of the SWL is composed of the η_{NTR}, while during the 100 year event, 17% of the SWL is composed of η_{NTR} (Figure 3). This change in the composition of the SWL is driven by larger elevation η_{SS} during the 100 year TWL event. Representative stations (Toke Point, WA; South Beach, OR; San Francisco, CA; and La Jolla, CA) display a shift in the distribution of η_{SS} toward larger magnitudes during the 100 year TWL event, while η_{MMSLA} and η_{SE} distributions stay similar to that of the annual maximum event (Figure 4). As the contribution of η_{SS} to the SWL increases during the 100 year TWL event, the contribution of the $\eta_A + \eta_{MSL}$ decreases from 90.5% ($\pm$5.7%) to 82.0% ($\pm$4.8%), while contributions from η_{SE} and η_{MMSLA} change by 1% or less.

4. Discussion

A compound event framework, relevant for TWLs on beaches, focuses on impacts contingent on multiple, statistically dependent variables [*Leonard et al.*, 2014]. Short records preclude a full understanding of how individual processes combine to drive extreme TWLs, preventing adequate descriptions of realizable events. Synthetic TWL records allow for the extraction of low-probability return level events and therefore provide insight into the makeup of extreme coastal water levels not previously captured by observed records. Results indicate that the magnitude of the individual components contributing to the 100 year TWL event are less than the 100 year event of the individual component (i.e., the 100 year Hs is not driving the 100 year TWL). Therefore, a 100 year compound extreme TWL is a combination of variables that are not necessarily extreme events in and of themselves.

4.1. Regional Variability of Extreme Total Water Levels

Differences in the magnitude of the TWL components is due to regional controls on water levels. Overall, the $R_{2\%}$ contributes just as much, and often more, to extreme TWLs as the SWL. The magnitude of $R_{2\%}$ has a latitudinal dependence, where $R_{2\%}$ in Washington and Oregon is almost 1 m larger than $R_{2\%}$ in Southern California. This is largely a reflection of the wave climate; Hs during the annual maximum TWL is 3 m larger in Astoria, OR, than in La Jolla, CA (Figure S1). The peak in wave height in northern/central Oregon is likely due to onshore winds directed toward the Oregon coast during major storm events [*Allan and Komar*, 2006]. Tp during the annual maximum TWL event is 2 s longer in the south than the north, which dampens some of the regional variation in $R_{2\%}$. This suggests that extreme TWLs in California have a tendency to coincide with slightly longer period swell.

Extreme SWLs on the U.S. West Coast tend to be tidally dominated [*Merrifield et al.*, 2013]. Tides are mixed (predominantly semidiurnal) and the tidal range is classified as mesotidal north of San Francisco, CA, and microtidal south of San Francisco, CA. Tides are largest in southern Washington and decrease southward (Table S1). The quasi 4.4 year cycle (from the 8.85 year cycle of lunar perigee) contributes the most to semidiurnal regions [*Haigh et al.*, 2011], and ranges from 5 to 10 cm, decreasing moving north to south. The range of the 18.61 year lunar nodal cycle contributes less to high water levels along the U.S. West Coast and increases 3–5 cm north to south.

η_{NTR} also displays latitudinal dependence, peaking at Toke Point, WA, and decreasing toward the south. The majority of this latitudinal variability in η_{NTR} during extreme TWL events is driven by η_{SE} and η_{SS}, while the elevation of η_{MMSLA} only varies by a few centimeters (Figure S1). In Washington and Oregon, η_{SE} tends to be lowest in the summer due to coastal upwelling, where cold waters depress local sea level [*Komar and Enfield*, 1987; *Huyer*, 1983]. In the winter, water levels are elevated due to thermal expansion and the geostrophic effects of currents. South of Point Conception in Southern California, η_{SE} is negative, thus reducing the elevation of the TWL (Figure S1). Winds are relatively weak, and the recirculation of the California Current drives variations in upwelling and downwelling cycles with a less clear signal than the Pacific Northwest coastline [*Huyer*, 1983], causing negative seasonal anomalies in the winter when storm surges predominate. η_{SS}, the largest driver of the η_{NTR} elevation, decreases in magnitude from Washington to California (Figure S1). Most of this latitudinal variation reflects dominant paths of storms crossing the North Pacific [*Favre and Gershunov*, 2006; *Graham and Diaz*, 2001]; however, gradients north and south of Toke Point suggest that more processes are at work. Larger tidal ranges along the Canadian coastline [*Haigh et al.*, 2011] coupled with a slightly larger wave climate due to storms from the Gulf of Alaska [*Reguero et al.*, 2012] suggest that TWLs to the north may be larger than those in northern Washington.

While the most extreme waves occur in Washington and Oregon, $R_{2\%}$ is on average a larger contributor to both the annual maximum and the 100 year TWL event in central California. This is coincident with the lowest tidal ranges and some of the smallest η_{NTRs} in the region. In Southern California, the SWL becomes the largest contributor due to less frequent storm systems [*Graham and Diaz*, 2001], a more southerly oriented coastline which shelters the coast from Gulf of Alaska storms [*Seymour*, 2011], and offshore islands and complex nearshore bathymetry that locally alters wave conditions [*O'Reilly and Guza*, 1993]. η_{MMSLA} is not a large contributor to the annual maximum or 100 year TWL event; however, it decreases in magnitude slightly from mid-Oregon to Southern California.

4.2. Variability in Still Water Levels During Extreme Total Water Levels

Daily maximum TWLs usually occur during the highest tide of the day [*Serafin and Ruggiero*, 2014]; therefore, it is not surprising that the contribution from $\eta_A + \eta_{MSL}$ is less during the 100 year TWL event than the annual maximum event: As the TWL magnitude increases, the elevation of the tide does not (Figure 3). Our approach treats η_{SE} as deterministic, based on the historical climatology of the region. Therefore, both the annual maximum and 100 year TWL events are most likely to occur during the winter [*Menéndez and Woodworth*, 2010]. Consequently, the magnitude and relative contribution of η_{SE} is similar across both extreme event scenarios.

Perhaps most surprising is the minimal change in the relative contribution of η_{MMSLAs} to the 100 year TWL event, revealing that elevated η_{MMSLAs} alone are not necessary for extreme return level events. El Niño events drive anomalous increases in η_{MMSLAs} for months at a time [*Komar et al.*, 2011; *Allan and Komar*, 2002] and coastal impacts from strong El Niño events have been well documented along the U.S. West Coast [*Barnard et al.*, 2015, 2011]. Our results indicate that the 100 year TWL event is not always concurrent with El Niños and occurs during both high and low η_{MMSLA}. While elevated η_{MMSLAs} may increase the TWL over some threshold to drive erosion and flooding, their magnitude, even during anomalously high years, is much smaller than η_{SS}.

The most extreme η_{SS} events on the U.S. West Coast are usually between 0.5 and 1.5 m making it seem less important to flooding and erosion when compared with the U.S. East Coast, where η_{SS} can reach as much as 10 m during major hurricanes [*Fritz et al.*, 2007]. However, even η_{SS} of over 1 m can drive tens of meters of erosion on low-sloping beaches [*Allan et al.*, 2011]. Our results suggest that less frequently occurring TWL return level events are driven by η_{SS} due to the tail of the distribution (Figure 4). In contrast, η_{SE} and η_A are bounded by their deterministic nature and η_{MMSLAs} over 15 cm (a reasonable estimate for high anomalies) occur on average (standard deviation) 10% (6%) of the time during the annual maximum TWL event and 7% (4%) during the 100 year TWL event. Therefore, less frequent return level events are most likely driven by less bounded components, such as η_{SS}.

4.3. Validity of Assumptions and Areas of Future Research

Our simulation approach assumes that the amplitude of the η_{SE} and η_A are deterministic. However, studies have described temporal changes in both of these components. *Wahl et al.* [2014] discovered an amplification of the annual signal from 1990 onward in the Gulf of Mexico, while *Mawdsley et al.* [2015] and *Jay* [2009] determined tidal amplitudes have increased and may continue to increase with further rises in η_{MSL}. While our assumptions produce little difference in the magnitude of these components between the annual maximum and the 100 year TWL event, changes to η_A and η_{SE} may be important to consider with increases in sea level.

In order to focus on the large-scale, hydrodynamic drivers of extreme TWL events, our work utilizes a realistic, yet regionally uniform, estimate of β across the U.S. West Coast. However, wave runup is strongly dependent on the variability of coastal morphology and β [*Cohn and Ruggiero*, 2016]. Beach slope and coastal morphology experience temporal and spatial variability [*Di Leonardo and Ruggiero*, 2015; *Larson and Kraus*, 1994], making wave runup a highly site specific parameter. Future studies will investigate sites across the U.S. West Coast with high-resolution morphology data in order to explore how variations in β and both shelf and nearshore bathymetry may further influence regional differences in the composition of extreme TWLs.

Understanding the present-day contribution of individual components to extreme TWLs will help to better interpret how future large-scale changes to the climate may affect regional drivers of coastal flooding and erosion. While there is still a fairly high level of uncertainty, future projections of wave climate downscaled from global climate models [*Erikson et al.*, 2015; *Wang et al.*, 2014; *Hemer et al.*, 2013] predict changes to storminess along the U.S. West Coast. Increases or decreases to Hs, Tp, or the angle of storm impact may have a larger influence in locations where the $R_{2\%}$ is the largest contributor to the TWL. Future changes to η_{SS} are not as well studied along the U.S. West Coast; however, their contribution to the SWL on average doubles during higher

TWL return level events. While SLR will ultimately be the largest contributor to increases in coastal flooding and erosion events by the end of the century, changes to storminess may dictate differences in extreme TWL return level events over the next few decades.

5. Conclusions

This study provides a characterization of the variability in the magnitude and relative contributions to extreme TWLs at the shoreline along the U.S. West Coast. The magnitude of extreme TWLs peak in southwest Washington and decrease to the south. This regional variability is driven by a combination of differences in tidal ranges, patterns of storminess, and seasonal cycles. Differences also exist in the relative contribution of individual components to extreme TWL events, where central California is more influenced by wave-induced water levels than Washington and Oregon. However, Washington and Oregon's larger tidal range and nontidal residuals constitute a large percentage of the contribution to TWLs in these locations. Using a probabilistic simulation technique, we evaluate less frequent, yet more extreme, TWL return level events and find an increase in event magnitude driven by slight increases in wave runup and a doubling of the contribution of storm surge to the TWL. Understanding how individual processes combine to drive extreme TWLs along U.S. West Coast beaches will help decipher where future changes to the global climate may most dramatically affect regional coastal flooding and erosion.

Acknowledgments

Tide gauge records are available through the National Oceanic and Atmospheric Administration (NOAA) National Ocean Service (NOS) website. We thank Melisa Menéndez and Jorge Pérez at the Environmental Hydraulics Institute of the Universidad de Cantabria (IHCantabria) for providing the Global Ocean Wave 2 (GOW2) data. We also thank Thomas Wahl, Nathaniel Plant, and an anonymous reviewer for their reviews and constructive comments. This work was funded by the U.S. Geological Survey, the NOAA Coastal and Ocean Climate Applications (COCA) program (NA12OAR4310195), the NOAA Regional Integrated Sciences and Assessments Program (RISA) (NA15OAR4310145), and the Strategic Environmental Research and Development Program (SERDP) (RC-2644).

References

Allan, J. C., and P. D. Komar (2002), Extreme storms on the Pacific Northwest coast during the 1997–98 El Niño and 1998–99 La Niña, *J. Coastal Res.*, *18*, 175–193.

Allan, J. C., and P. D. Komar (2006), Climate controls on US West Coast erosion processes, *J. Coastal Res.*, *22*, 511–529.

Allan, J. C., P. D. Komar, and P. Ruggiero (2011), Storm surge magnitudes and frequency on the central Oregon coast, in *Proceedings of the 2011 Solutions to Coastal Disasters Conference*, edited by L. Wallendorf et al., pp. 43–64, Am. Soc. Civ. Eng., Reston, Va., doi:10.1061/41185(417)6.

Barnard, P. L., J. C. Allan, J. E. Hansen, G. M. Kaminsky, P. Ruggiero, and A. Doria (2011), The impact of the 2009–10 El Niño Modoki on US West Coast beaches, *Geophys. Res. Lett.*, *38*, L13604, doi:10.1029/2011GL047707.

Barnard, P. L., et al. (2015), Coastal vulnerability across the Pacific dominated by El Niño/Southern Oscillation, *Nat. Geosci.*, *8*(10), 801–807.

Bromirski, P. D., R. E. Flick, and D. R. Cayan (2003), Storminess variability along the California coast: 1858–2000, *J. Clim.*, *16*(6), 982–993.

Chelton, D. B., and R. E. Davis (1982), Monthly mean sea-level variability along the west coast of North America, *J. Phys. Oceanogr.*, *12*(8), 757–784.

Church, J. A., and N. J. White (2011), Sea-level rise from the late 19th to the early 21st century, *Surv. Geophys.*, *32*(4–5), 585–602.

Church, J. A., et al., (2013), Sea level change, Tech. Rep., PM Cambridge Univ. Press.

Cohn, N., and P. Ruggiero (2016), The influence of seasonal to interannual nearshore profile variability on extreme water levels: Modeling wave runup on dissipative beaches, *Coastal Eng.*, *115*, 79–92.

Coles, S. (2001), *An Introduction to Statistical Modeling of Extreme Values*, Springer, London.

Di Leonardo, D., and P. Ruggiero (2015), Regional scale sandbar variability: Observations from the US Pacific Northwest, *Cont. Shelf Res.*, *95*, 74–88.

Dangendorf, S., A. Arns, J. G. Pinto, P. Ludwig, and J. Jensen (2016), The exceptional influence of storm "Xaver" on design water levels in the German Bight, *Environ. Res. Lett.*, *11*(054001).

Erikson, L. H., C. Hegermiller, P. Barnard, P. Ruggiero, and M. van Ormondt (2015), Projected wave conditions in the Eastern North Pacific under the influence of two CMIP5 climate scenarios, *Ocean Model.*, *96*, 171–185.

Favre, A., and A. Gershunov (2006), Extra-tropical cyclonic/anticyclonic activity in North-Eastern Pacific and air temperature extremes in western North America, *Clim. Dyn.*, *26*(6), 617–629.

Fritz, H. M., C. Blount, R. Sokoloski, J. Singleton, A. Fuggle, B. G. McAdoo, A. Moore, C. Grass, and B. Tate (2007), Hurricane Katrina storm surge distribution and field observations on the Mississippi barrier islands, *Estuarine Coastal Shelf Sci.*, *74*(1), 12–20.

Graham, N. E., and H. F. Diaz (2001), Evidence for intensification of North Pacific winter cyclones since 1948, *Bull. Am. Meteorol. Soc.*, *82*(9), 1869–1893.

Haigh, I. D., M. Eliot, and C. Pattiaratchi (2011), Global influences of the 18.61 year nodal cycle and 8.85 year cycle of lunar perigee on high tidal levels, *J. Geophys. Res.*, *116*, C06025, doi:10.1029/2010JC006645.

Hemer, M. A., Y. Fan, N. Mori, A. Semedo, and X. L. Wang (2013), Projected changes in wave climate from a multi-model ensemble, *Nat. Clim. Change*, *3*(5), 471–476.

Holman, R. A., and A. Sallenger (1985), Setup and swash on a natural beach, *J. Geophys. Res.*, *90*(C1), 945–953.

Huyer, A. (1983), Coastal upwelling in the California current system, *Prog. Oceanogr.*, *12*(3), 259–284.

Jay, D. A. (2009), Evolution of tidal amplitudes in the eastern Pacific Ocean, *Geophys. Res. Lett.*, *36*, L04603, doi:10.1029/2008GL036185.

Komar, P. D., and D. B. Enfield (1987), Short-term sea-level changes and coastal erosion, in *Sea-Level Fluctuation and Coastal Evolution: Society of Economic Paleontologists and Mineralogists Special Publication*, vol. 41, edited by N. Dag, H. P. Orrin, and D. H. James, pp. 17–27.

Komar, P. D., J. C. Allan, and P. Ruggiero (2011), Sea level variations along the U.S. Pacific Northwest coast: Tectonic and climate controls, *J. Coastal Res.*, *27*(5), 808–823.

Larson, M., and N. C. Kraus (1994), Temporal and spatial scales of beach profile change, Duck, North Carolina, *Mar. Geol.*, *117*(1), 75–94.

Leonard, M., S. Westra, A. Phatak, M. Lambert, B. van den Hurk, K. McInnes, J. Risbey, S. Schuster, D. Jakob, and M. Stafford-Smith (2014), A compound event framework for understanding extreme impacts, *WIREs Clim. Change*, *5*, 113–128.

Mawdsley, R. J., I. D. Haigh, and N. C. Wells (2015), Global secular changes in different tidal high water, low water and range levels, *Earth's Future*, *3*(2), 66–81.

Melet, A., R. Almar, and B. Meyssignac (2016), What dominates sea level at the coast: A case study for the Gulf of Guinea, *Ocean Dyn.*, *66*(5), 623–636.

Méndez, F. J., M. Menéndez, A. Luceño, and I. J. Losada (2006), Estimation of the long-term variability of extreme significant wave height using a time-dependent Peak Over Threshold (POT) model, *J. Geophys. Res.*, *111*, C07024, doi:10.1029/2005JC003344.
Méndez, F. J., M. Menéndez, A. Luceño, and I. J. Losada (2007), Analyzing monthly extreme sea levels with a time-dependent GEV model, *J. Atmos. Oceanic Technol.*, *24*(5), 894–911.
Méndez, F. J., C. Izaguirre, C. Menéndez, B. G. Reguero, and I. J. Losada (2010), Is the extreme wave climate in the NE Pacific increasing?, in *Oceans 2010 MTS/IEEE Seattle*, pp. 1–7, Institute of Electrical and Electronics Engineers, Seattle, Wash., doi:10.1109/OCEANS.2010.5664314.
Menéndez, M., and P. L. Woodworth (2010), Changes in extreme high water levels based on a quasi-global tide-gauge data set, *J. Geophys. Res.*, *115*, C10011, doi:10.1029/2009JC005997.
Merrifield, M. A., A. S. Genz, C. P. Kontoes, and J. J. Marra (2013), Annual maximum water levels from tide gauges: Contributing factors and geographic patterns, *J. Geophys. Res. Oceans*, *118*, 2535–2546, doi:10.1002/jgrc.20173.
Nerem, R., D. Chambers, C. Choe, and G. Mitchum (2010), Estimating mean sea level change from the TOPEX and Jason altimeter missions, *Mar. Geodesy*, *33*(S1), 435–446.
O'Reilly, W., and R. T. Guza (1993), A comparison of two spectral wave models in the Southern California bight, *Coastal Eng.*, *19*(3), 263–282.
Pérez, J., M. Menéndez, P. Camus, F. J. Méndez, and I. J. Losada (2015), Statistical multi-model climate projections of surface ocean waves in Europe, *Ocean Model.*, *96*, 161–170.
Pugh, D. T. (1996), Tides, surges and mean sea-level: A handbook for engineers and scientists.
Ray, R. D., and G. Foster (2016), Future nuisance flooding at Boston caused by astronomical tides alone, *Earth's Future*, *4*, 578–587, doi:10.1002/2016EF000423.
Reguero, B., M. Menéndez, F. Méndez, R. Mínguez, and I. Losada (2012), A Global Ocean Wave (GOW) calibrated reanalysis from 1948 onwards, *Coastal Eng.*, *65*, 38–55.
Ruggiero, P., P. D. Komar, W. G. McDougal, J. J. Marra, and R. A. Beach (2001), Wave runup, extreme water levels and the erosion of properties backing beaches, *J. Coastal Res.*, *17*(2), 407–419.
Ruggiero, P., P. D. Komar, and J. C. Allan (2010), Increasing wave heights and extreme value projections: The wave climate of the U.S. Pacific Northwest, *Coastal Eng.*, *57*(5), 539–552.
Sallenger, A. H. (2000), Storm impact scale for barrier islands, *J. Coastal Res.*, *16*, 890–895.
Serafin, K. A., and P. Ruggiero (2014), Simulating extreme total water levels using a time-dependent, extreme value approach, *J. Geophys. Res. Oceans*, *119*, 6305–6329, doi:10.1002/2014JC010093.
Seymour, R. J. (2011), Evidence for changes to the Northeast Pacific wave climate, *J. Coastal Res.*, *27*(1), 194–201.
Smith, R. L. (1986), Extreme value theory based on the R largest annual events, *J. Hydrol.*, *86*(1–2), 27–43.
Stockdon, H. F., R. A. Holman, P. A. Howd, and A. H. Sallenger Jr. (2006), Empirical parameterization of setup, swash, and runup, *Coastal Eng.*, *53*(7), 573–588.
Stockdon, H. F., A. H. Sallenger Jr, R. A. Holman, and P. A. Howd (2007), A simple model for the spatially-variable response to hurricanes, *Mar. Geol.*, *238*(1), 1–20.
Sweet, W. V., and J. Park (2014), From the extreme to the mean: Acceleration and tipping points of coastal inundation from sea level rise, *Earth's Future*, *2*(12), 579–600.
Tebaldi, C., B. H. Strauss, and C. E. Zervas (2012), Modelling sea level rise impacts on storm surges along US coasts, *Environ. Res. Lett.*, *7*(1), 014032.
Theuerkauf, E. J., A. B. Rodriguez, S. R. Fegley, and R. A. Luettich (2014), Sea level anomalies exacerbate beach erosion, *Geophys. Res. Lett.*, *41*, 5139–5147, doi:10.1002/2014GL060544.
Wahl, T., F. M. Calafat, and M. E. Luther (2014), Rapid changes in the seasonal sea level cycle along the US Gulf Coast from the late 20th century, *Geophys. Res. Lett.*, *41*, 491–498, doi:10.1002/2013GL058777.
Wahl, T., N. G. Plant, and J. W. Long (2016), Probabilistic assessment of erosion and flooding risk in the northern Gulf of Mexico, *J. Geophys. Res. Oceans*, *121*, 3029–3043, doi:10.1002/2015JC011482.
Wang, X. L., Y. Feng, and V. R. Swail (2014), Changes in global ocean wave heights as projected using multimodel CMIP5 simulations, *Geophys. Res. Lett.*, *41*, 1026–1034, doi:10.1002/2013GL058650.
Young, I., S. Zieger, and A. Babanin (2011), Global trends in wind speed and wave height, *Science*, *332*(6028), 451–455.